レーザー非定常作用による超音速圧力場の変調に関する数値・実験研究

酒井　武治*1　中村　佳朗*2　佐宗　章弘*3　松田　淳*4

Nomenclature

p = pressure, Pa
Q = laser energy, J
r = radial distance, m
r_0 = radius of v_0, m
S = heating source term by laser energy deposition, J/m^3
T = temperature, K
t = time, s
v_0 = spherical volume for laser energy deposition, m^3
x = axial distance, m
η = ratio of an absorbed laser energy to a deposited energy
ρ = density, kg/m^3
τ = Laser duration time, s

Subscripts

s = stagnation point on the centerline of the blunt body
$s0$ = stagnation point on the centerline of the blunt body for the case of the steady state without energy deposition

I. INTRODUCTION

Developing a flow control technique by using a pulse laser has been paid much attention recently. A number of past works have shown that the aerodynamic drag force on the body flying at supersonic speed can be reduced by supplying pulse laser energy in a supersonic flow. (see e.g. the review article by Knight *et al.*[1]) In the method, the drag decreases unsteadily during the interaction of the high temperature plasma created by the laser energy with the shock wave over the supersonic body. Therefore, a deep understanding of the effect of the energy supply on the reduction of the pressure on the wall of the body is necessary in order to apply this technique practically.

Extensive efforts have been made to understand the unsteady interaction of the laser induced plasma generated by the energy supply using a single laser pulse. Despite such efforts, the effect of the energy deposition on the drag reduction is not satisfactorily understood. Georgievsky and Levin[2] studied the interaction of a thermal region with a sphere in a freestream Mach number of 3 through the numerical simulation by using a computational fluid dynamic (CFD) method. In the numerical simulation, the thermal region was set to be a constant low density zone upstream of the shock wave over the sphere. The results showed that the stagnation point pressure of the sphere was reduced during the interaction of the thermal region with the shock wave. After the value of the stagnation point pressure had a minimum value, the pressure returned to its steady state value after reverberating compression and expansion. Adelgren *et al.*[3] experimentally investigated the interaction of a high temperature plasma with the shock wave over a sphere in a freestream Mach number of 3.45. The plasma was produced by using a pulsed Nd: YAG laser. The time history of the pressure at the stagnation point on the sphere was measured. Inde-

＊1　名古屋大学大学院 工学研究科航空宇宙工学専攻　講師（代表者）
＊2　名古屋大学大学院 工学研究科航空宇宙工学専攻　教授
＊3　名古屋大学大学院 工学研究科航空宇宙工学専攻　教授
＊4　名古屋大学大学院 工学研究科航空宇宙工学専攻　助教

pendently, calculations were carried out to analyze the unsteady flowfield in the Adelgren *et al.*'s experimental condition.[4,5] The calculated time history of the pressure contradicted the measured one: The two expansion regions where the pressure was below its steady state one were seen in the calculated time history, following the interaction of the plasma with the bow shock wave over the sphere. However, the measured time history of the pressure showed only one expansion region. It should be noted that such two expansions were seen in the calculated result obtained by Georgievsky and Levin.[2] The reason for the discrepancy seen in the time history of the pressure between measurement and calculation remains unknown.

In the present study, an experimental and numerical study is conducted to understand the time evolution of the flowfield during the interaction of the laser-induced plasma with the shock wave over a blunt body in a supersonic flow. Efforts are firstly made to give a satisfactory explanation on the time evolution of the interacting flowfield, and on the time history of the pressure at the stagnation point of the blunt body between experiment and calculation. A better agreement is obtained between the experiment and the calculation in the present study. Next, based on the reasonable agreement, the time history of the drag of the body is calculated by using the calculated pressure distribution over the body. Finally, the averaged drag reduction and the total reduction of the impulse during the interaction are evaluated by using the time history of the drag.

The time evolution of the interacting flowfield with the laser-induced plasma is examined only for one experimental condition in the present study. The laser parameters such as pulsing frequency, duration time, and laser energy will have a strong impact on the unsteady flowfield structure and the time history of the flow properties on the blunt body. The examination of such a effect is out of the scope of the present work. Such a task will be required for a deep understanding of the interacting flowfield using a pulse laser, and will be planned in future. As stated, there is a discrepancy between experiment and calculation even if a simulated condition is matched in the experiment and calculation. This work serves partially to validate the simulated parameter chosen in the present work.

II. EXPERIMENT CONFIGURATION

An indraft supersonic wind tunnel is used in the experiment. A schematic diagram of the experimental setup is shown in Fig. 1. The Mach number and the static pressure of the flow is estimated to be 3.0 and 3kPa, respectively. A test model has a flat-faced cylindrical shape with a diameter of 17 mm. During the experiment, the flowfield is visualized by using a Schlieren optical setup and a high speed camera.

A laser pulse is supplied from an upstream location through the wind tunnel nozzle by using a Nd:YAG laser with the laser wavelength of 1,064 nm. The temporal distribution of the Nd:YAG laser pulse is given in Fig. 2. The full width of half maximum for a pulse is 9 ns and the total energy supplied during a pulse is set to be 0.45 J. The spatial distribution of the laser pulse is not measured. However, we have confirmed the repeatability that the shape of the plasma so created is nearly spherical under the present experimental condition. Therefore, the effect of the spatial distribution on the shock wave generation is believed to be small within the condition considered in the present study.

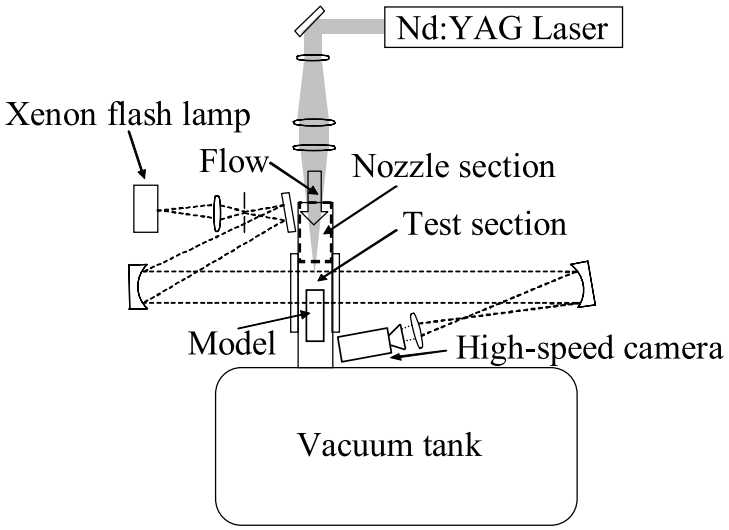

Fig. 1 A schematic diagram of experimental setup

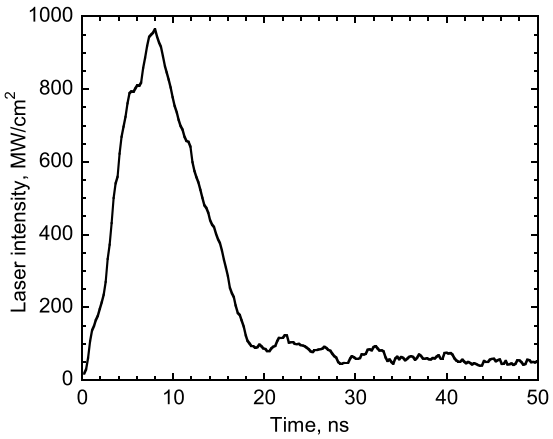

Fig. 2 Temporal distribution of a Nd: YAG laser with the laser wavelength of 1,064 nm

The laser beam is focused at a point in the centerline of the wind tunnel flow about 40 mm away from the stagnation point of the test model. Even if the focusing point is reduced about 10%, the experimental result shows a nearly similar trend. Thus, the focusing point chosen in the present study will have little effect on the result presented in this work. However, we could not examine the effect of the larger distance of the focusing point from the body because the flow region which is available for the laser beam focusing is limited in the current nozzle geometry.

A piezoelectric pressure transducer is used to measure the time variation of the pressure at the stagnation point of the test model. The pressure transducer is flush-mounted on the test model. Unfortunately, because the possible temperature variation during measurement is out of range for the pressure transducer used in the present study, the sensitivity of the measured pressure value is not calibrated. Therefore, the experimental data is mainly used to compare the time variation of the stagnation point pressure, not the absolute value of the pressure, between experiment and calculation, as will be shown later.

III. METHOD OF CALCULATION

A computational fluid dynamic method is used to simulate the experimental condition. The 2d-axisymmetric inviscid flow is assumed to be a perfect gas with the constant specific heat ratio of 1.4. Mass, momentum, and energy conservation equations are discretized using a finite-volume method. The numerical flux function is evaluated using the AUSM-DV scheme.[6] The MUSCL approach with a minmod limiter is used to improve the spatial accuracy by setting the artificial compression parameter to be 1. Computed flow properties are second-order accurate in space. The discretized equations are numerically integrated in time by using a second-order Runge-Kutta method. Note that the present numerical method is a modified version of the multi-dimensional flow code which has already been applied to analyze the high speed and high temperature flow problems over a blunt body.[7]

A heating source term by the pulsed laser energy deposition is calculated assuming that the energy is deposited during the period of the order of the laser pulse duration at constant volume and that the deposited energy distribution is given by a Gaussian profile. A well-known formulation[5] for the energy deposition is used in the present study as follows:

$$S(x, r, t) = \rho\lambda(t) q_0 \exp\left[-\left(\frac{(x-x_0)+r^2}{r_0^2}\right)\right]$$

where $\lambda(t)$ denotes a step function

$$\lambda(t) = \begin{Bmatrix} 1, & 0 < t < \tau \\ 0, & t > \tau \end{Bmatrix}$$

The value of q_0 is given by the following relation:[5]

$$q_0 = \frac{\eta Q}{\rho\tau \int_{\upsilon_0} \exp\left[-\left(\frac{(x-x_0)+r^2}{r_0^2}\right)\right] d\upsilon}$$

Because the absorbed energy volume, υ_o, could not be determined in the experiment, the value of this volume is assumed to be the same value of 3 mm^3 used in the past work.[5] Calculation is carried out by using the volume value of 6 mm^3. The result shows that the computed time history for the pressure at the centerline of the blunt body is not so changed between υ_o=3 mm^3 and υ_o=6 mm^3. The ratio of an absorbed energy to a deposited energy, η, is determined by reproducing the time evolution of the diameter for the blast shock wave evaluated by the Schlieren photographs taken in the experiment before the blast shock wave is reached at the wall. The fitted value for η becomes 0.08.

Other numerical procedures are as follows: The static temperature in the freestream is calculated through an isentropic flow relation assuming that the total temperature of the freestream is taken to be 300 K; A slip condition is imposed at the wall of the blunt body; The computed results are presented by using a 201 × 401 computational grid; Note that the calculation with a 301 × 501 grid does not change the flowfield structures and the stagnation point pressure value appreciably. The computational domain is shown in Fig. 3. The computational parameters are summarized in Table 1.

IV. RESULTS AND DISCUSSION

A. Computed time history of the pressure at the stagnation point

In Fig. 4, the computed pressure at the stagnation point of the flat-faced cylinder is plotted against the time from t = 0 to 300 μs. On the vertical axis, the computed pressure value is normalized by the steady state value without energy deposition. From the figure, a first sharp increase is seen at about t = 40 μs. After this first increase, the pressure value is reduced. A second increase is observed at about t = 90 μs. The second reduction of the pressure value is recognized until t = 105 μs. The third pressure increase is followed by the second reduction, and the pressure value is returning to its original value gradually. A similar trend is seen in a previous work,[4,5] though the calculation was made for the flowfield over a sphere. The comparison of the unsteady flowfield at each time shown in the figure will be made next.

Table 1 Computational parameters

Parameter	Value
Specific heat ratio	1.4
Freestream pressure, Pa	3000
Freestream temperature, K	107
Freestream Mach number	3
CFL number	0.1
Diameter of flat-faced cylinder, mm	17.
Q, J	0.45
r_0, m	9.0×10^{-4}
η	0.08
τ, s	9.0×10^{-9}
Artificial compression（MUSCL）	1

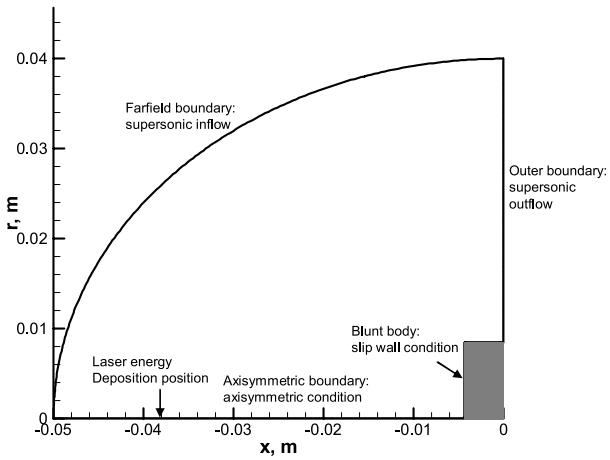

Fig. 3 Computational domain and the related boundary conditions

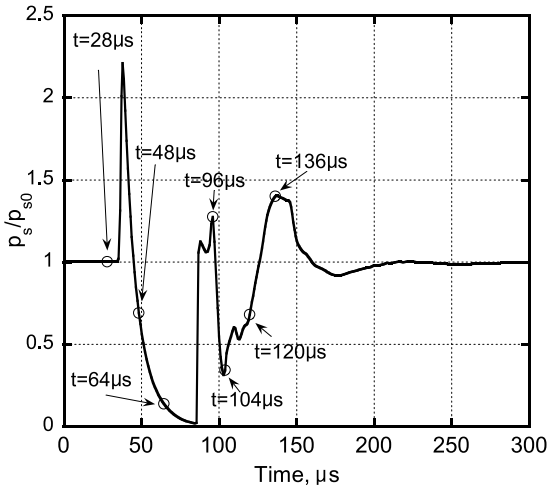

Fig. 4 Calculated time evolution of the stagnation point pressure at the centerline of the flat-faced cylindrical blunt body

B. Comparison of flowfield between experiment and calculation

Figures 5 (a) – (e) show the Schlieren photograph, the calculated density, pressure and temperature contours at t = 28 μs, respectively. The temperature contour will be given hereafter because it is useful to trace the laser induced plasma, although the calculated temperature value obtained by the present ideal gas computation may differ from the experimental one. From the figures, it is found that the blast wave reaches at the bow shock wave over the body. The position of the blast wave agrees between experiment and calculation. In addition, for reference, the values of the density, pressure, and temperature along the centerline of the blunt body normalized by each of the stagnation point value for the case of the steady state value without laser energy deposition are given in Fig. 5 (e). One can see that the diameter of the nearly spherical high temperature region produced by the laser energy deposition is about 1 cm.

In Figs. 6 (a) – (e), the Schlieren photograph, the calculated contours, and the centerline properties at t = 48 μs are given respectively. The figures give the flowfield structure after the reflection of the blast shock wave. The blast wave starts to be reflected on the wall at about t = 36 μs, as was expected from the sharp pressure increase shown in Fig. 4. When a bow shock wave interacts with the high temperature region created by the laser energy deposition, the shape of the bow shock wave is deformed due to the decrease of the local Mach number.[2] The deformed bow shock wave is also seen in Figs. 6 (b), and (c), respectively. One can see in Figs. 6 (b), and (d) that the shape of the thermally heated region near the centerline is transformed drastically. From Fig. 6 (e), the thickness of the thermally heated region is about 5 mm. It should be also noted that the thermally heated region totally entered in the shock layer at this time. As a result of the interaction of the bow shock wave with the thermal region, a rarefaction wave propagates towards the wall surface of the blunt body and the rarefac-

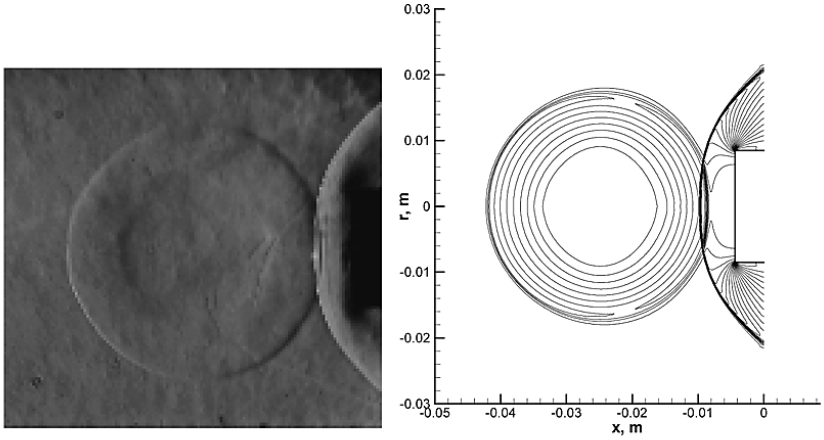

(a) Schlieren photograph (b) Density contour

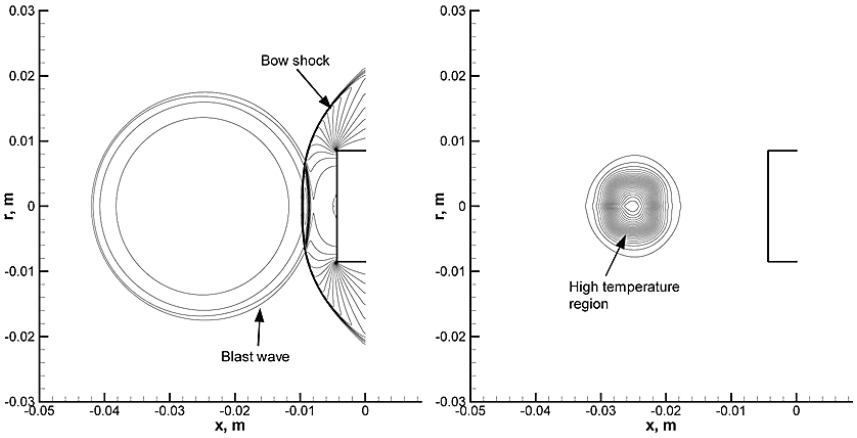

(c) Pressure contour (d) Temperature contour

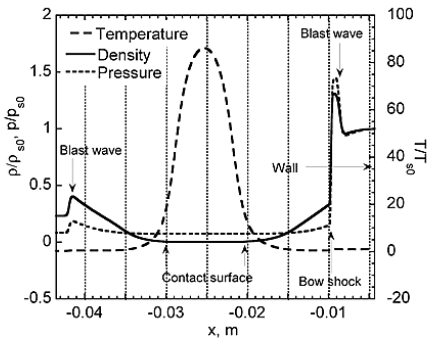

(e) Calculated density, pressure, and temperature distribution along centerline, the properties are normalized by the steady state value without laser energy deposition

Fig. 5. Comparison of unsteady flowfield at t = 28 μs

tion wave reduces the wall pressure.[2] This trend can be confirmed in Fig. 4, and also from the comparison of the pressure distribution near the wall between Fig. 5 (e) and Fig. 6 (e). In addition, though the result is not shown, a reversal flow from the wall to the main freestream is produced in the shock layer. This flow tends to compress the gas in the region between the deformed bow shock and the reflected blast wave, as will be shown later. In addition, the flow in this region is accelerated up to a supersonic speed. As a result, a shock wave is formed. One can see this shock wave in Fig. 6 (c), which is denoted by 'SW1'. The SW1 is observed as a small increase in the pressure distribution shown in Fig. 6 (e). A distorted contact surface can be barely seen in Fig. 6 (a) ahead of the light region adjacent to the frontal wall of the blunt body. The observed flow structure is likely to be consistent with the calculated density contour given in Fig. 6 (b).

The results at t = 64 μs are shown in Figs. 7 (a) – (e), respectively. These results indicate that the high pressure region is produced in the region between the deformed bow shock wave and the SW1. After this time, the SW1 moves to the wall surface and is reflected at the wall. The arrival of the SW1 on the wall represents the second rise of the stagnation point pressure at about t = 90 μs as shown in Fig. 4. Note that a similar phenomenon is reported in the previous numerical study.[5] The isopycnics for both calculation and experiment agree well each

other: one can see the two light zones in Fig. 7 (a) and, the zones are interpreted as the two shock waves seen in the calculated results. Meanwhile, one can expect from the temperature contour in Fig. 7 (d) that the vortices are generated, though the details are not shown here. The vortices are believed to be produced mainly due to the baroclinic effect[8] followed by the interaction of the shock wave with the thermal heated region. From Fig. 7 (e), the region between the two light zones at the centerline is believed to be equivalent to that between the show shock waves denoted by 'Deformed shock wave' and 'SW1' in the figure. The thickness in the region at the centerline is found to be about 4 mm.

The next results are given at t = 96μs in Figs. 8 (a) – (e), respectively. It should be noted in Fig. 8 (e) that the range of the scales in the horizontal coordinate and in the normalized temperature is reduced compared with the previous figures shown in Figs. 5 (e), 6 (e), and 7 (e). The results show that the SW1 is reflected at the wall, and is interacting with the thermal region. As a result of the interaction of the SW1 with the thermal region, the stagnation point pressure begins to decrease due to the effect of the rarefaction fan, as was seen in the interaction of the thermal region with the bow shock wave. The effect is recognized as the second reduction of the stagnation point pres-

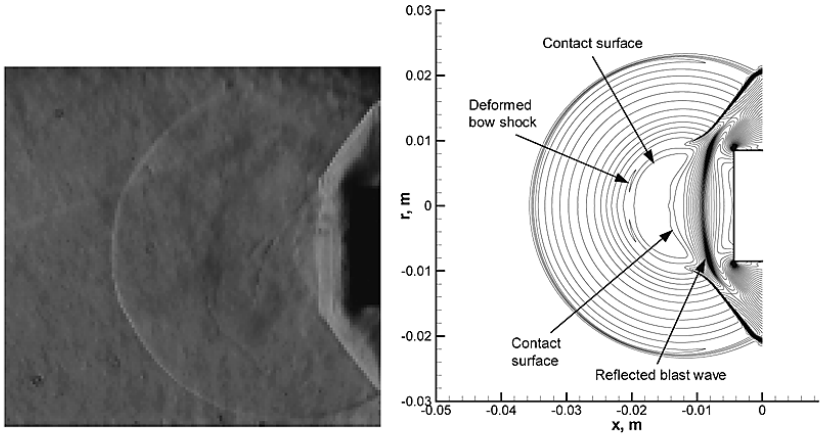

(a) Schlieren photograph (b) Density contour

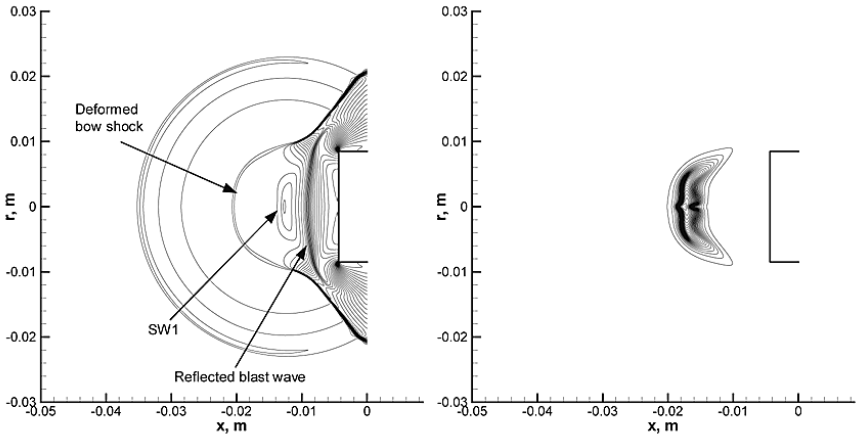

(c) Pressure contour (d) Temperature contour

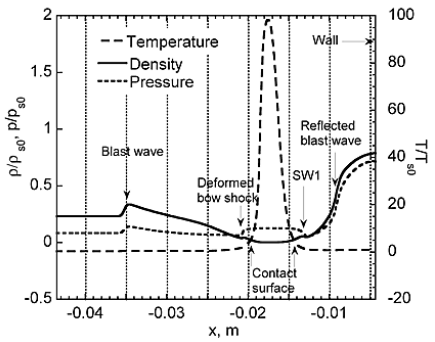

(e) Calculated density, pressure, and temperature distribution along centerline, the properties are normalized by the steady state value without laser energy deposition

Fig. 6. Comparison of unsteady flowfield at t = 48 μs

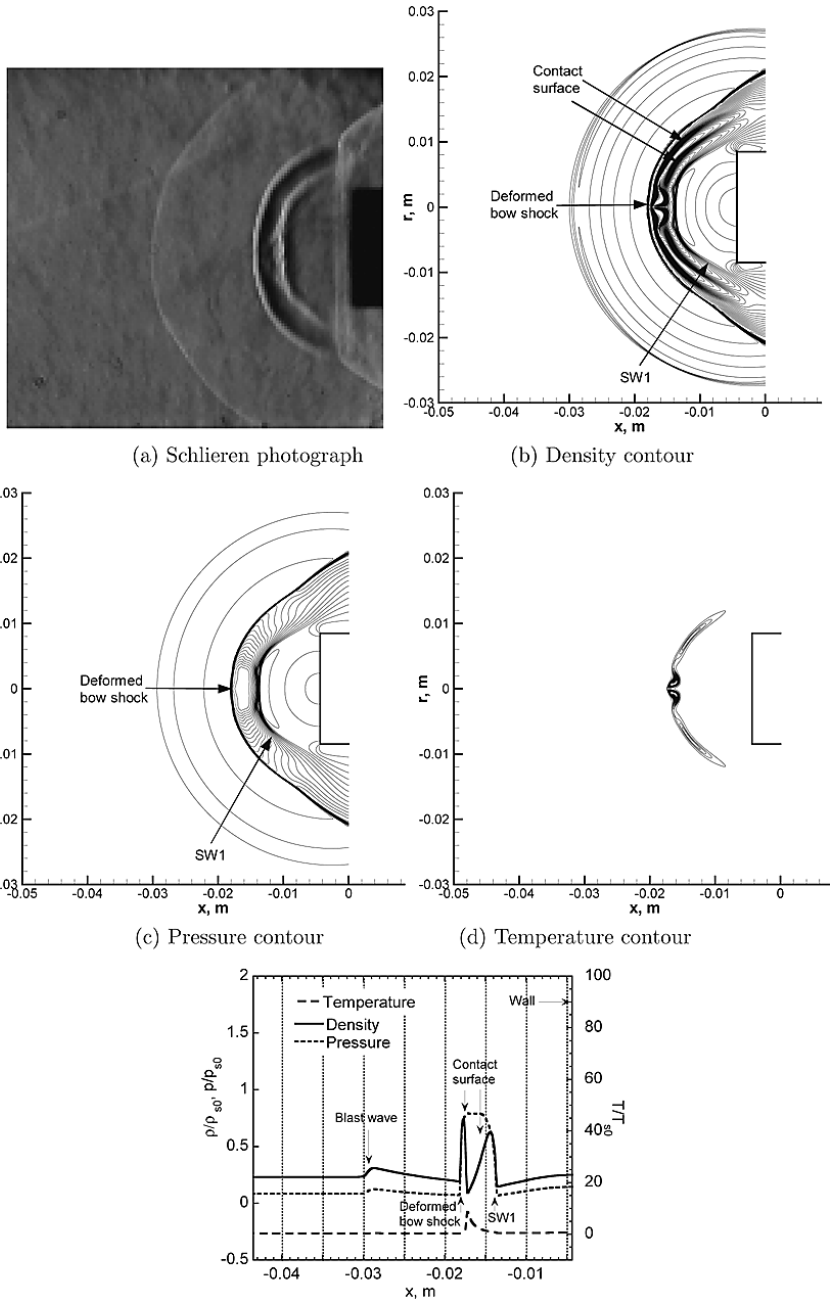

(a) Schlieren photograph (b) Density contour

(c) Pressure contour (d) Temperature contour

(e) Calculated density, pressure, and temperature distribution along centerline, the properties are normalized by the steady state value without laser energy deposition

Fig. 7. Comparison of unsteady flowfield at t = 64 μs

sure shown in Fig. 4. From Figs. 8 (b) and 8 (d), it is found that the thermal region is convected to the wall surface, and is stretched out in the freestream direction. In addition, the thermal region is limited within two spots. The spots are placed in the off-centerline region as can be surmised from Fig. 8 (e) in which one cannot find any high temperature region between 'Contact surface' and 'Reflected SW1' denoted in the figure. The normalized temperature is about 10 at most within the spots. From the pressure contour given in Fig. 8 (c), one can confirm that the high temperature spot is relatively small: the deformation of SW1 is represented by the twin small bumps and the shock wave near the centerline moves slowly to an upstream region compared with the twin bumps. A dark line is seen in Fig. 8 (a). The dark line is believed to be the contact surface shown in Fig. 8 (b).

From Figs. 8 (a), and 8 (b), the position of the calculated blast wave is closer to the deformed bow shock wave as compared with the experimental result: the calculated thickness at the centerline between the two waves is about 2.5 mm as is shown in Fig. 8 (e). The cause of the difference is due to the fact that a thermochemical nature in the heated region by laser energy deposition is different between experiment and calculation. The bow shock wave will be differently deformed depending on the thermochemical state of the laser-induced plas-

ma. However, the effect of the downstream part of the blast wave on the stagnation point pressure will be negligibly small. Note that the calculated results in the previous works[4,5] show that the time history of the stagnation point pressure is not so changed between an ideal gas and a high temperature real gas model.

The third compression starts after about t = 100 μs. Figures 9 (a) – (e) show the results at t = 104 μs. At this time, the SW1 passes entirely through the thermal spots on the off-centerline, as can be seen in Fig 9 (b). The thermal spots are distorted again and the contact surface is transformed into doubly blooming shape, as is shown in Fig. 9 (d). Because of the two bumps on the reflected SW1 shown in Fig. 8 (c), it is believed that the reflected SW1 focuses at three local region as is indicated in Fig. 9 (c). As a result of the shock wave focusing, the pressure behind the reflected SW1 becomes high. The increase in the pressure distribution by the shock wave focusing can be seen as a small bump between 'Wall' and 'Reflected SW1' shown in Fig. 9 (e). The calculated result indicates that the third increase starts when this pressure wave produced by the focusing reaches at the wall.

Regardless of the pressure wave propagation by the focusing so predicted, the main contribution to the third compression is attributed to

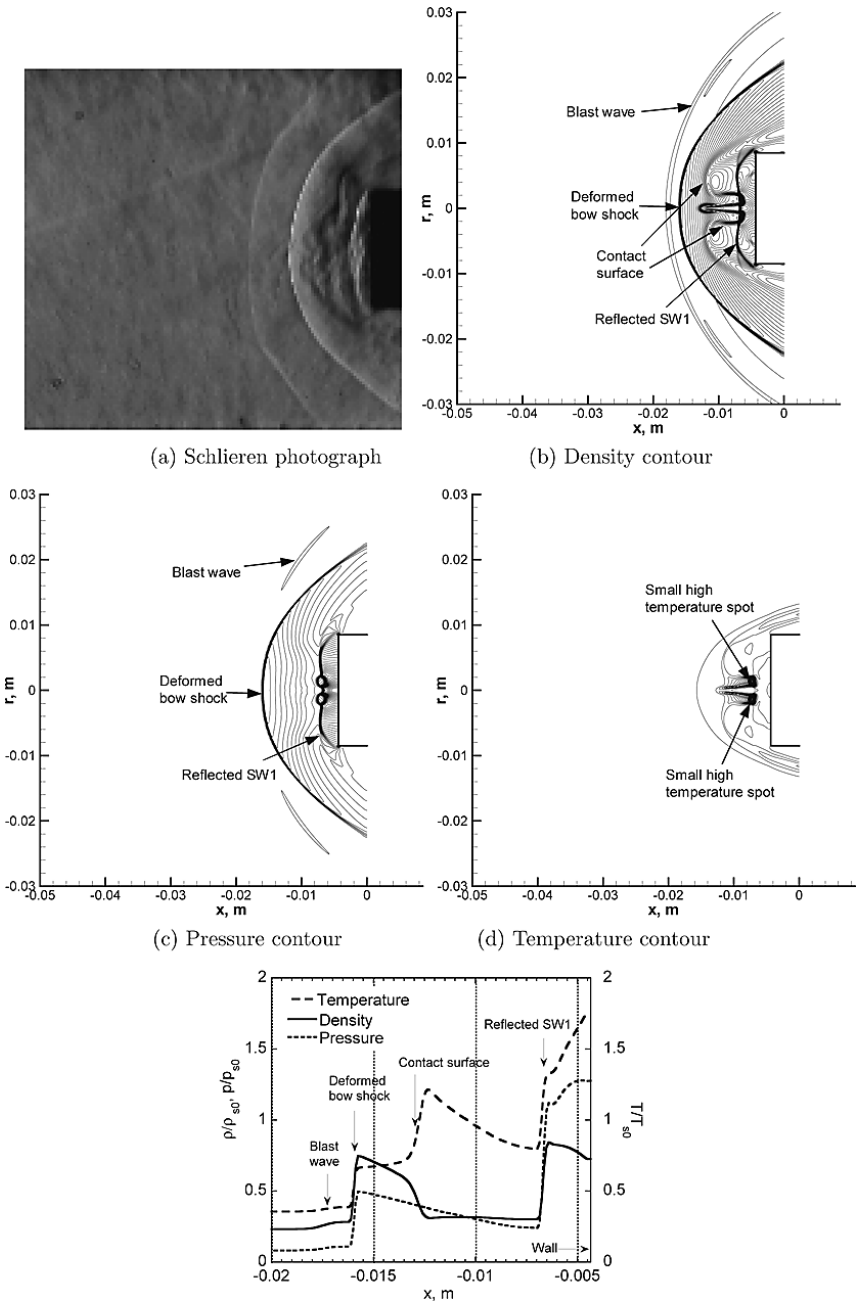

(a) Schlieren photograph (b) Density contour

(c) Pressure contour (d) Temperature contour

(e) Calculated density, pressure, and temperature distribution along centerline, the properties are normalized by the steady state value without laser energy deposition

Fig. 8. Comparison of unsteady flowfield at t = 96 μs

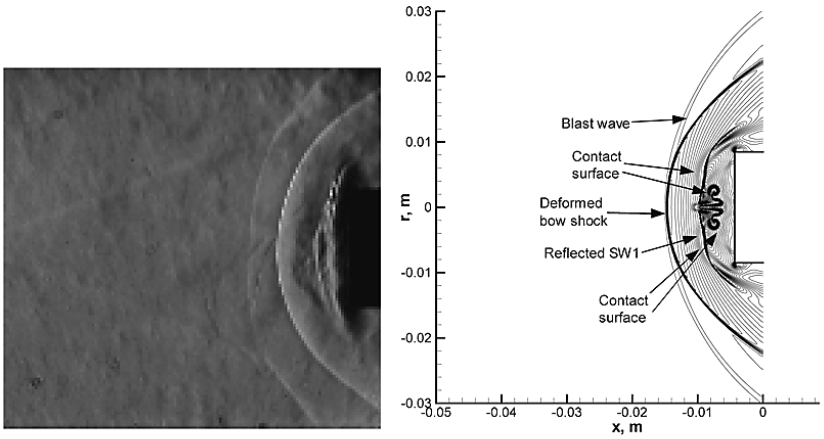

(a) Schlieren photograph (b) Density contour

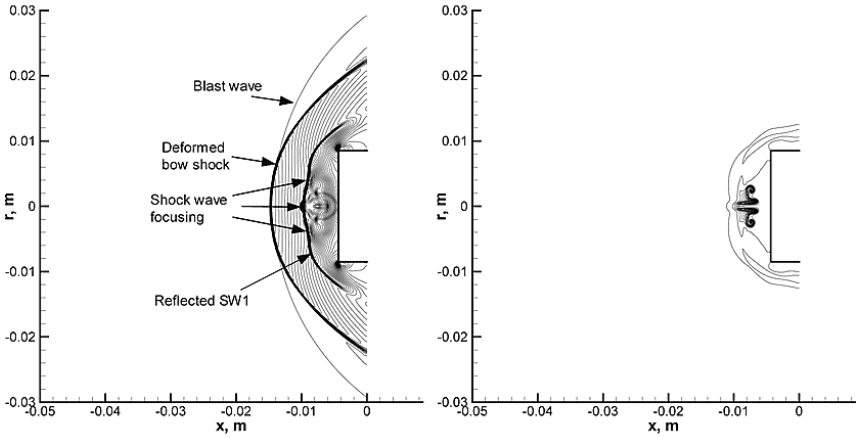

(c) Pressure contour (d) Temperature contour

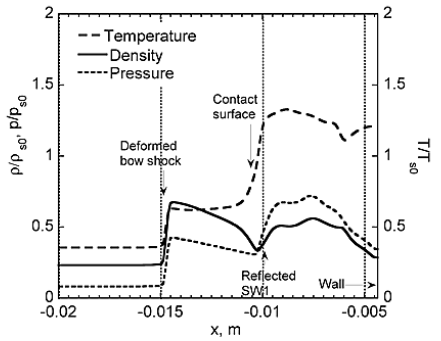

(e) Calculated density, pressure, and temperature distribution along centerline, the properties are normalized by the steady state value without laser energy deposition

Fig. 9. Comparison of unsteady flowfield at t = 104 μ s

the recover of the deformed shock wave at its steady state position for the case analyzed in the present study. This trend was already reported in the previous work.[3–5] Figures 10 (a) – (e) show the results at t = 120 μs. It is found that from Figs.10 (a) – (c) that the deformed bow shock wave is approaching to the frontal surface of the blunt body. In addition, the compression wave is seen in Fig. 10 (c). The compression at the centerline near the wall region can be confirmed also from Fig. 10 (e). From the Schlieren photograph given in Fig. 10 (a), the two discontinuous waves are observed, as expected. These waves presumably correspond to the deformed shock wave and the reflected SW1 shown in Figs.10 (b) and (c).

Lastly, the results at t = 136 μs are presented in Figs. 11 (a) – (e), respectively. At this time, the pressure at the stagnation point becomes about 1.4 times higher than the steady state value. The relatively large increase occurs when the bow shock wave reaches at the position closer to the wall compared with the steady state case. The experimental result shown in Fig. 11 (a) implies this trend qualitatively. The shock thickness at the centerline is found to be reduced by about 15% from the comparison between Fig. 5 (e) and Fig. 11 (e). After this time, the flowfield structure over the blunt body gradually returns to its steady-state one, as was shown in Fig. 4. One can see in Figs. 11

(b), and (d) that the energy deposited region remains in the flow region adjacent to the frontal surface of the blunt body even at this time. The region affects the pressure distribution only slightly. However, this region could cause higher heat fluxes on the wall.[4] The heat flux distribution needs to be examined, and this task will be made in the future.

C. Comparison of pressure at the stagnation point between experiment and calculation

In Fig. 12, the time history of the stagnation point pressure of the flat-faced cylinder is compared between measurement and calculation. The present calculation showed that the minimum temperature at the stagnation point becomes about 100 K during the first decrease in the time history of the pressure at the stagnation point. Since the temperature is out of the range of the pressure transducer calibration, the experimental value is fitted to the numerical one. A good agreement of the temporal variation of the pressure is seen between the measurement and calculation. This agreement confirms the qualitative description of the flowfield structure explained earlier.

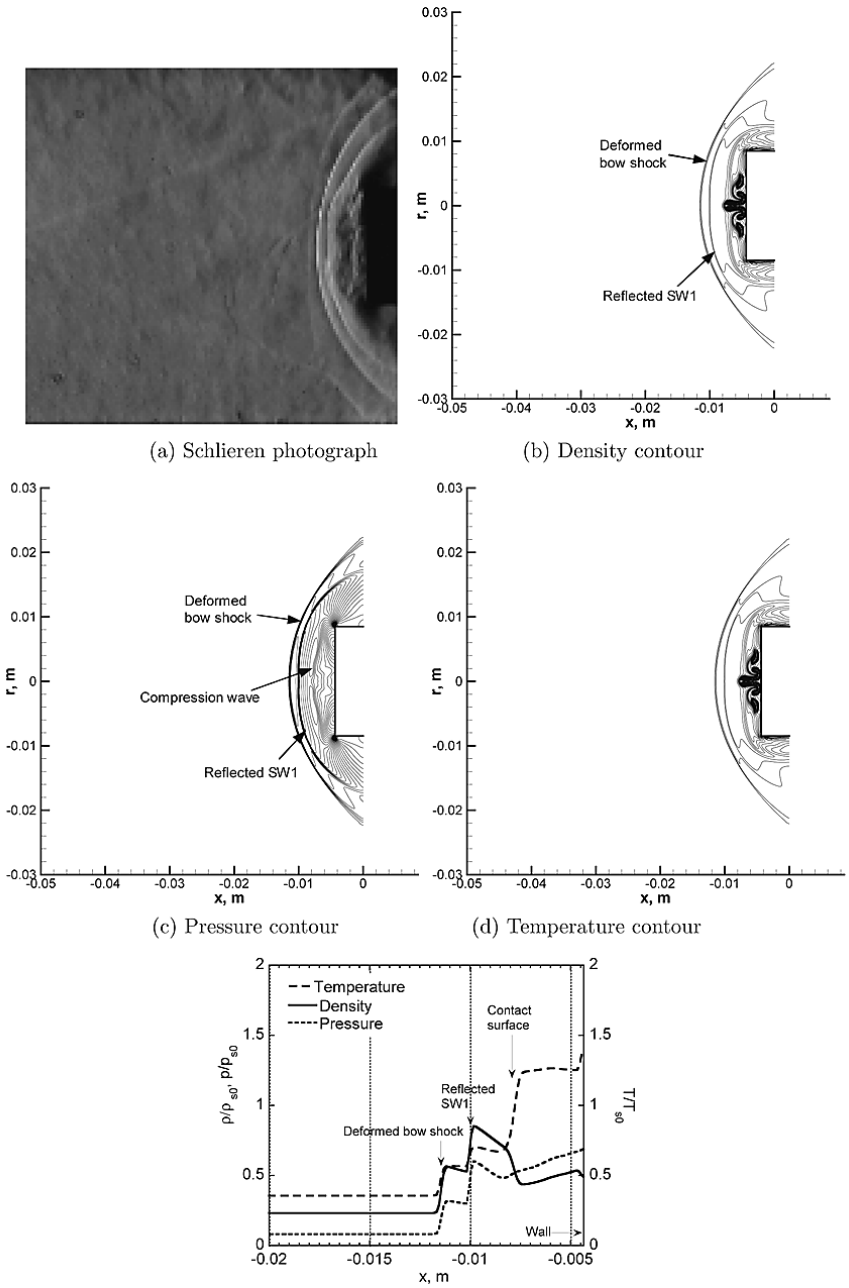

(a) Schlieren photograph (b) Density contour

(c) Pressure contour (d) Temperature contour

(e) Calculated density, pressure, and temperature distribution along centerline, the properties are normalized by the steady state value without laser energy deposition

Fig. 10. Comparison of unsteady flowfield at t = 120 μ s

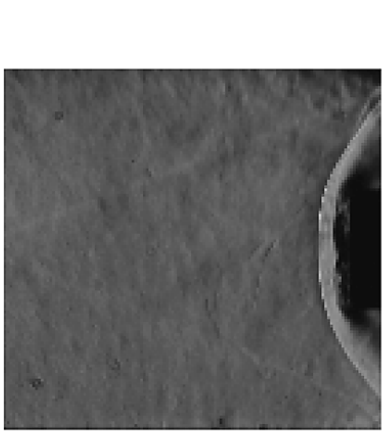

(a) Schlieren photograph

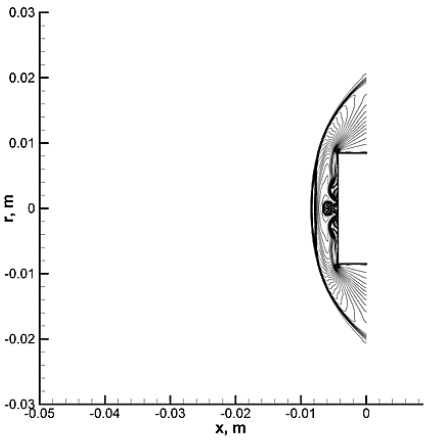

(b) Density contour

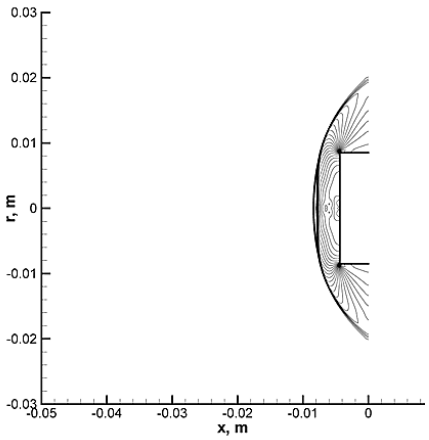

(c) Pressure contour

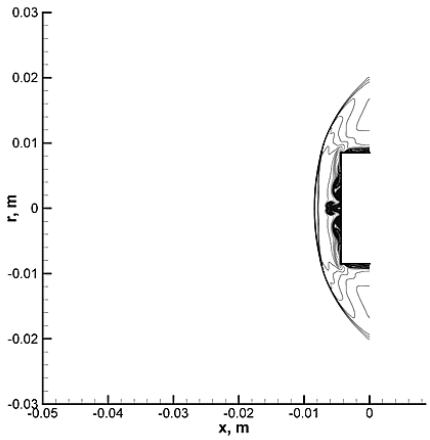

(d) Temperature contour

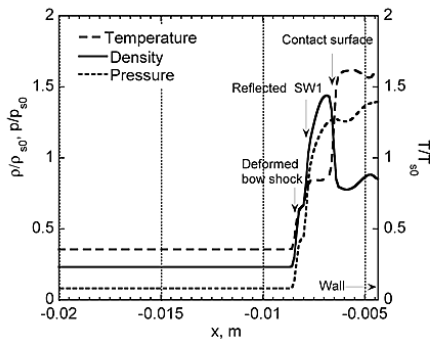

(e) Calculated density, pressure, and temperature distribution along centerline, the properties are normalized by the steady state value without laser energy deposition

Fig. 11. Comparison of unsteady flowfield at t = 136 μ s

D. Drag Reduction

Figure 13 shows the time variation of the drag on the frontal surface of the cylindrical body is plotted against the elapsed time. The drag value on axis of ordinate is normalized by the one for the steady state case. The drag at each time is calculated by integrating the pressure along the frontal area of the wall. From the figure, the reduction of the drag continues for about 80 μs from about t = 45 to 125 μs. The calculated result shows that the pressure value on the most of the off-centerline region along the body is lower than the steady state value during the second increase of the stagnation point pressure, though the result is not given here. The lower surface pressure in the off-centerline region results in the lower drag value than the steady-state one during the second increase, as is shown in Fig. 13. The averaged drag over the period from t = 0 to 250 μs, which is supposed to be the end of the interaction, becomes about 86% of its the steady-state value.

The impulse is calculated by integrating the drag value on the frontal surface given in Fig. 13 with time until 250 μs. By subtracting the calculated impulse value from the steady-state one, the total reduction of the impulse value is estimated to be about 5.3×10^{-4}kg・m/s. The reduction of the impulse value during the period from the first peak in the pressure history to the second one attributes to the total

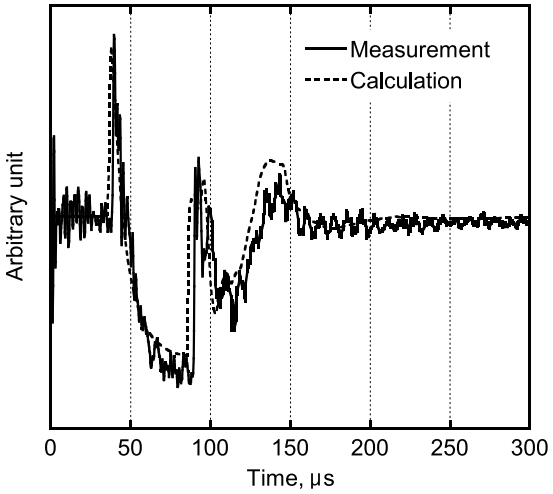

Fig. 12. Comparison of time history of the stagnation point pressure at the centerline of the flat-faced cylinder between measurement and calculation

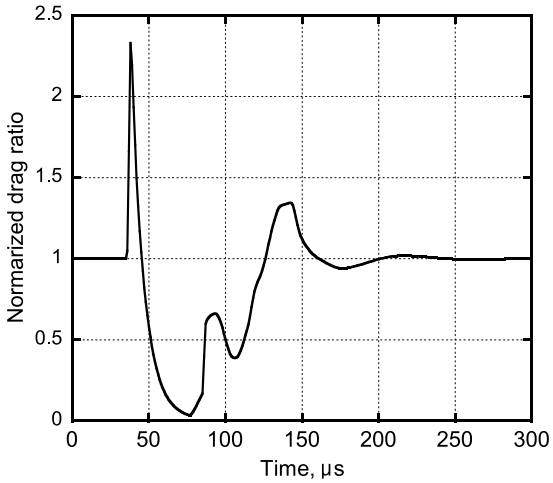

Fig. 13. Time history of the drag excreted on the frontal surface of the flat-faced cylinder

reduction by about 70%. Even though the second and third compressions are observed after that period, the total impulse value is moderately reduced and its contribution to the total reduction becomes about 30% on the average.

V. CONCLUDING REMARKS

An experimental and numerical study is made for the interaction of the shock wave with the thermal energy region created by laser energy deposition in a supersonic flow over a flat-faced cylindrical blunt body. The density fields agree well between the experiment and the calculation. By combining the experimental and the numerical results, the drag reduces by about 86% compared with the steady-state one on the average during the effective interaction time of 250 μs deduced for a single pulse laser energy deposition in the present study.

ACKNOWLEDGMENTS

The authors would like to thank Mr.Yohei Sekiya, who is a graduate student of this department, for his energetic accomplishment to conduct the experiemnt throughout this project.

REFERENCES

1 Knight D., Kuchinskiy V., Kuranov, A., and Sheikin, E., “Survey of Aerodynamic Flow Control at High Speed By Energy Deposition,” AIAA Paper 2003-0525, January, 2003.

2 Georgievsky, P., and Levin, V., “Unsteady Interaction of a Sphere with Atmospheric Temperature Inhomogeneity at Supersonic Speed,” *Mekhanika Zhidkosti i Gaza*, No.4, May-June 1993, pp. 174–183 (in Russian); translated in *Fluid Dynamics*, Vol.28, No.4, 1993, pp. 568–574.

3 Adelgren, R. A., Yan, H., Elliott G. S., Knight D. D., Beutner T. J., and Zheltovodov, A. A., “Control of Edney IV Interaction by Pulsed Laser Energy Deposition,” *AIAA Journal*, Vol. 43, No. 2, 2005, pp. 256–269.

4 Kandala, R., and Candler G. V., “Numerical Studies of Laser-Induced Energy Deposition for Supersonic Flow Control,” *AIAA Journal*, Vol. 42, No. 11, 2004, pp. 2266–2275.

5 Zheltovodov, A. A., Pimonov, E. A., and Knight D.D., “Energy Deposition Influence on Supersonic Flow Over Axisymmetric Bodies,” AIAA Paper 2007–1230, January, 2007.

6 Wada, Y., and Liou, M. S., “A Flux Splitting Scheme with High-Resolution and Robustness for Discontinuities,” AIAA paper 94–0083, January, 1994.

7 Sakai T., and Sawada, K., “Calculation of Nonequilibrium Radiation from a Blunt Body Shock Layer,” *Journal of Thermophysics and*

Heat Transfer, Vol. 17, No. 1, January-March 2003, pp. 21–28.

8 Sasoh, A, Ohtani, T., and Mori, K., “Pressure Effects in a Shock-Wave–Plasma Interaction Induced by a Focused Laser Pulse,” *Physical Review Letters*, Vol. 97, No. 20, Art. No. 205004, November 2006.